From Bistate Molecular Switches to Self-Directed Track-Walking Nanomotors

Iong Ying Loh,[†,‡] Juan Cheng,[†,§] Shern Ren Tee,[†,§] Artem Efremov,[†] and Zhisong Wang[*,†,‡,§]

[†]Department of Physics, [‡]NUS Graduate School for Integrative Sciences and Engineering, [§]Center for Computational Science and Engineering, National University of Singapore, Singapore 117542. The manuscript was written through contributions of all authors. All authors have given approval to the final version of the manuscript.

ABSTRACT Track-walking nanomotors and larger systems integrating these motors are important for wide real-world applications of nanotechnology. However, inventing these nanomotors remains difficult, a sharp contrast to the widespread success of simpler switch-like nanodevices, even though the latter already encompasses basic elements of the former such as engine-like bistate contraction/extension or leg-like controllable binding. This conspicuous gap reflects an impeding bottleneck for the nanomotor development, namely, lack of a modularized construction by which spatially and functionally separable "engines" and "legs" are flexibly assembled into a self-directed motor. Indeed, all track-walking nanomotors reported to date combine the engine and leg functions in the same molecular part, which largely underpins the device—motor gap. Here we propose a general design principle allowing the modularized nanomotor construction from disentangled engine-like and leg-like motifs, and provide an experimental proof of concept by implementing a bipedal DNA nanomotor up to a best working regime of this versatile design principle. The motor uses a light-powered contraction—extension switch to drive a coordinated hand-over-hand directional walking on a DNA track. Systematic fluorescence experiments confirm the motor's directional motion and suggest that the motor possesses two directional biases, one for rear leg dissociation and one for forward leg binding. This study opens a viable route to develop track-walking nanomotors from numerous molecular switches and binding motifs available from nanodevice research and biology.

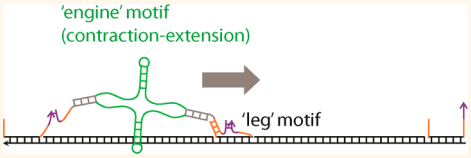

KEYWORDS: molecular machine · nanomotor · DNA · modular design · optomechanics

A key to advance the present nanotechnology toward wide real-world applications is to move from simple, switch-like nanodevices to integrated nanomachines[1−4] of extended functionalities. Self-propelled, self-directed track-walking nanomotors[5−18] may play a strategic role in this transition in a parallel to macroscopic heat engines and locomotives in the Great Industrial Revolution two centuries ago. More than a dozen track-walking nanomotors[5−18] have been reported to date, the majority of which are burn-the-bridge motors that gain a direction by either damaging the traversed track or denying an externally administered strand linking the part of track to a motor. Development beyond the first wave of burn-the-bridge motors is largely stagnant at present; only a few track-intact motors[11,12,16,17] have been reported, and their performance is far from comparable with biological nanowalkers[19−21] that inspire the artificial counterparts. A hard reality at the present stage is that the invention of track-walking nanomotors and related machine systems remains a difficult field accessible only to a small number of laboratories over the globe, which is a sharp contrast to the widespread research of bistate nanodevices that are switched between two well-defined states including different binding sites,[22−26] lengths,[27−32] molecular conformations,[33−36] binding affinity,[37,38] *etc.*

The gap between the motors and switching devices is conspicuous since many of these devices already qualify as nanoscale engines: they consume energy to generate a back-and-forth motion that in turn can drive other molecular processes. It is unclear how the many engine-like switching devices can be integrated with leg-like binding components to make motors in any general way, especially for motors beyond the burn-the-bridge ones. Virtually all artificial track-walking nanomotors[5−18] reported to date use their leg-like components not only for track-binding and gait control, but also

* Address correspondence to phywangz@nus.edu.sg.

Received for review June 27, 2014 and accepted September 30, 2014.

Published online September 30, 2014
10.1021/nn5034983

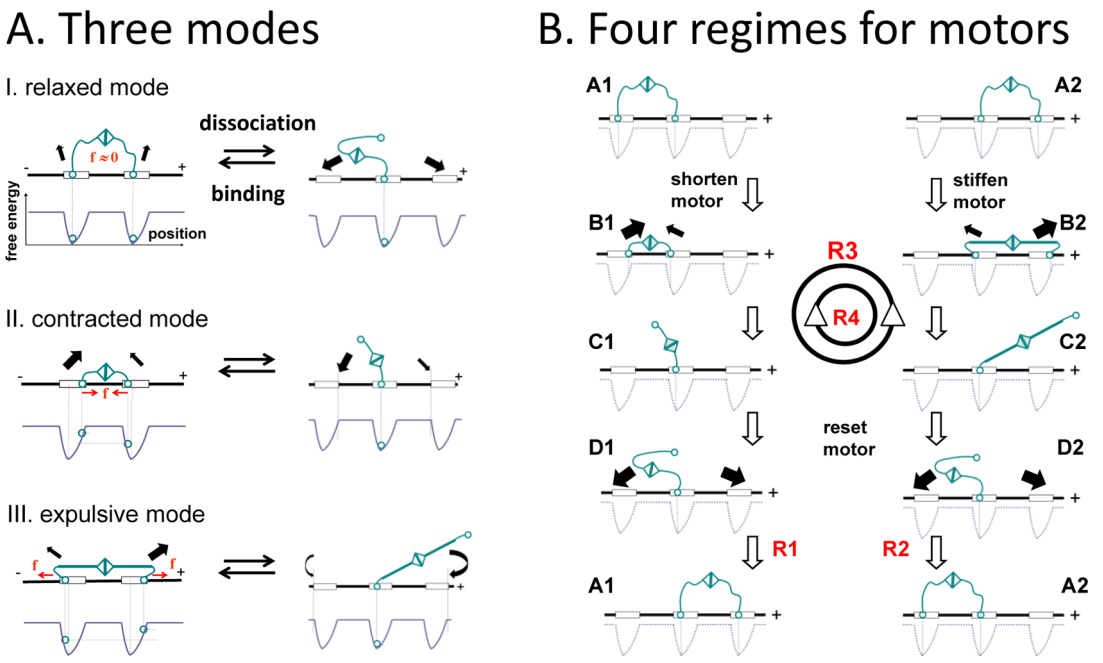

Figure 1. Design principle. (A) Three size-controlled modes of a symmetric bipedal nanomotor interacting with a periodic track of asymmetric binding sites. The motor and track are schematically illustrated in cyan and black; the underlying blue lines show the binding free energy between a motor leg (empty circle) and the binding sites (empty rectangles). A leg-site binding is asymmetric in that it is broken more easily when the leg is pulled by a force toward one end of the track than the other end. This asymmetry amounts to a binding free energy that changes more steeply along one edge than the other. As an example, the two edges are shown here as harmonic oscillator potentials with a lower elastic constant for the edge near the track's plus end as indicated. The size of a motor limits its leg-track interaction to different modes: a short motor (compared to the binding site period) explores the two inner edges of adjacent sites (contracted mode); a long motor explores the two outer edges. The same internal tension (f) of a two-leg bound motor causes more displacement along the less steep edge and does more work to raise the free energy, resulting in a lower barrier hence a higher rate for leg dissociation along this edge than the other one (higher rates indicated by larger size for bold, filled arrows). But the dissociated leg accesses the less steep edge more easily too, and binds the track along this edge by a higher rate. The dissociation and binding have opposite preference within either mode, yielding no net direction (detailed balance). (B) Multiple regimes for a unidirectional motor by switching it between the modes. The empty arrows indicate the operation cycles: A1 → B1 → C1 → D1 → A1 for regimes R1, A2 → B2 → C2 → D2 → A2 for R2, B1 → C1 → C2 → B2 → B1 for R3, and the reverse cycle for R4. For R1 and R2, the ending states of their cycles (A1, A2) are shown to have the motor in a different position from the starting states in order to reflect the motor's net direction. The leg binding forming the ending state (D1 → A1, D2 → A2) can occur either forward or backward by equal chance; the motor's net direction comes from the bias in the leg dissociation (B1 → C1, B2 → C2).

for energy consumption and force generation. But a single molecular component concentrating nearly all the technical requirements remains extremely difficult to make at this stage, hence the gap between the motors and devices. A modular design method is desirable by which a motor may be flexibly assembled from two functionally and spatially separable modular components: an engine or switch component responsible for energy consumption/force generation and a leg component responsible for track-binding and motion control. This modular design should be capable of rectifying back-and-forth motion of an engine or switch into continuous directional motion of a motor along its track. Such a modular design potentially opens a route to develop nanomotors from many switching nanodevices.

Hence lack of a modular motor design for separable and modularized engine- and leg-like components is a common impeding bottleneck at this early stage of nanomotor development. The highly tangled engine-leg is a feature largely borrowed from biological nanowalkers of kinesin[19] and myosin[20] families. However, another family of biological nanowalkers called dynein[21] keep the engine-like component distantly away from the track-binding component, and the same fuel-consuming engine component drives many nanomachines of diverse functions in living cells, suggesting possibility of modular designs for nanomotors. In the present study, we propose and experimentally demonstrate a versatile modular design principle by which walking nanomotors free of bridge burning may be flexibly formed from functionally and spatially separable leg-like components and bistate switches as the engine.

RESULTS

A Versatile Design Principle. The design principle, schematically illustrated in Figure 1, applies generally to nanomotors with two identical legs and tracks with periodic binding sites. A major requirement is an asymmetric leg-site binding: a track-bound leg is dissociated more easily (*i.e.*, with a higher rate) by a force

pulling the leg toward one end of the track (henceforth called plus end) than toward the opposite end (minus end). Then a symmetric motor can exploit the track's asymmetry in three distinctly different modes depending on the motor's size (Figure 1A, panels I–III).

When the motor's size (*i.e.*, its average leg-to-leg distance) matches the track's binding site period, a relaxed mode occurs in which the two-leg bound motor has a low internal tension. Then the motor's two legs have equal chance for dissociation by thermal fluctuation regardless of the track's asymmetry. When the motor's size is smaller than the binding site period, a contracted mode occurs in which the two-leg bound motor develops an inward tension to pull the leg near the plus end (called front leg henceforth) backward but pull the other leg (rear leg) forward. The opposite pulling dissociates the rear leg preferentially (*i.e.*, a higher dissociation rate for the rear leg than the front leg). When the motor is longer than the binding site period and is rigid, an expulsive mode occurs instead in which the motor's internal tension becomes outward to dissociate the front leg preferentially. Within each of the three modes alone, the motor has zero net direction as the detailed balance dictates that any site-selective preference for dissociation is balanced by an opposite preference for subsequent spontaneous binding of the dissociated leg. Hence the leg binding is preferred forward, backward and equal for both directions for the expulsive, contracted and relaxed modes, respectively. How the dissociation and binding preference can arise from a leg-site binding is explained in Figure 1.

Multiple regimes exist for making unidirectional motors by switching between the three modes to break the detailed balance. Four regimes are schematically illustrated in Figure 1B (marked from R1 to R4). For regime R1, alternately switching between the relaxed and contracted modes, *e.g.*, by changing the motor's size between two values, makes a repeatable cycle, in which the preference for rear leg dissociation in the contracted mode cannot be entirely compromised by the equal binding in the relaxed mode. This breaks the detailed balance to make a motor with a net direction toward the plus end. A motor with an opposite net direction is likewise made by switching between the relaxed and expulsive modes, *e.g.*, by changing the motor's rigidity. This is regime R2. The R1, R2 regimes have a directional preference for leg dissociation but not for leg binding. Alternately switching between the contracted and expulsive modes leads to two new regimes with double preference for both dissociation and binding. If the motor's two-leg bound state in the expulsive mode (B2 in Figure 1B) is more stable than that in the contracted mode (B1), it is more likely that the switch from the expulsive to contracted mode induces leg dissociation and the reverse switch induces leg binding. Alternating both switches then automatically selects regime R3 in which the operation cycle is a preferred rear leg dissociation followed by a preferred forward leg binding. If instead the two-leg state in the contracted mode is more stable, the same alternating switches select regime R4, resulting in a reversed operation cycle and an opposite direction of the motor. We note that regime R1 was previously discussed in a theoretical paper.[39]

Construction of a DNA Motor-Track Implementing the Modular Design Principle. All the four regimes allow construction of nanomotors from functionally and spatially separable "legs" and "engines": the former are a pair of identical legs responsible for an asymmetric binding with the track; the latter are a bistate switch changing the interleg bridge between two values of length or rigidity. Such a modular design is implemented in a light-powered DNA nanomotor, which is schematically illustrated in Figure 2.

The motor has two identical single-stranded legs connected by a light-switchable double-stranded bridge. Specifically, the bridge is a four-way junction between two engine-like hairpins embedded with light-responsive azobenzene and two spacer duplexes separating the engine and the legs. Alternating visible light and UV irradiations close and open the hairpins, thereby causing contraction and extension of the bridge. Such a light-controlled hairpin opening and closing have been demonstrated in ref 37, from which the sequence for the two 8-bp-long stems of one hairpin is taken. To immobilize the four-way junction for the motor's structural stability, the stem sequence for the other hairpin has a modified order for the same nucleotide and azobenzene contents. The track supports identical binding sites that each contains two overhangs for leg binding (Figure 2B). The motor and tracks with two or three binding sites were assembled from DNA strands by an annealing procedure (Materials and Methods), which largely follows previous studies[16,17] of DNA motors. The gel analysis of the annealed products yields one prominent band that is identified as the assembled motor or tracks (Figure 2C).

The asymmetric binding comes from the design feature that the two adjacent overhangs at a site, a 10-nt D1* overhang and a 20-nt D2*-plus-D1* overhang with the latter leading toward the track's plus end, compete to bind the motor's leg with complementary D1, D2 sequences (Figure 2D). A leg may hybridize simultaneously with both overhangs into D1-D1* and D2-D2* duplexes (both 10-bp long) as allowed by the length of the overhangs. But the duplex at the long overhang can grow to weaken the D1-D1* duplex at the short overhang. The D1-D1* weakening is decelerated or accelerated when the leg is pulled backward or forward *via* its D1 segment linking to the motor's main body. This gives rise to a preferential rear dissociation when a visible irradiation closes both hairpins to shrink the motor into a contracted mode.

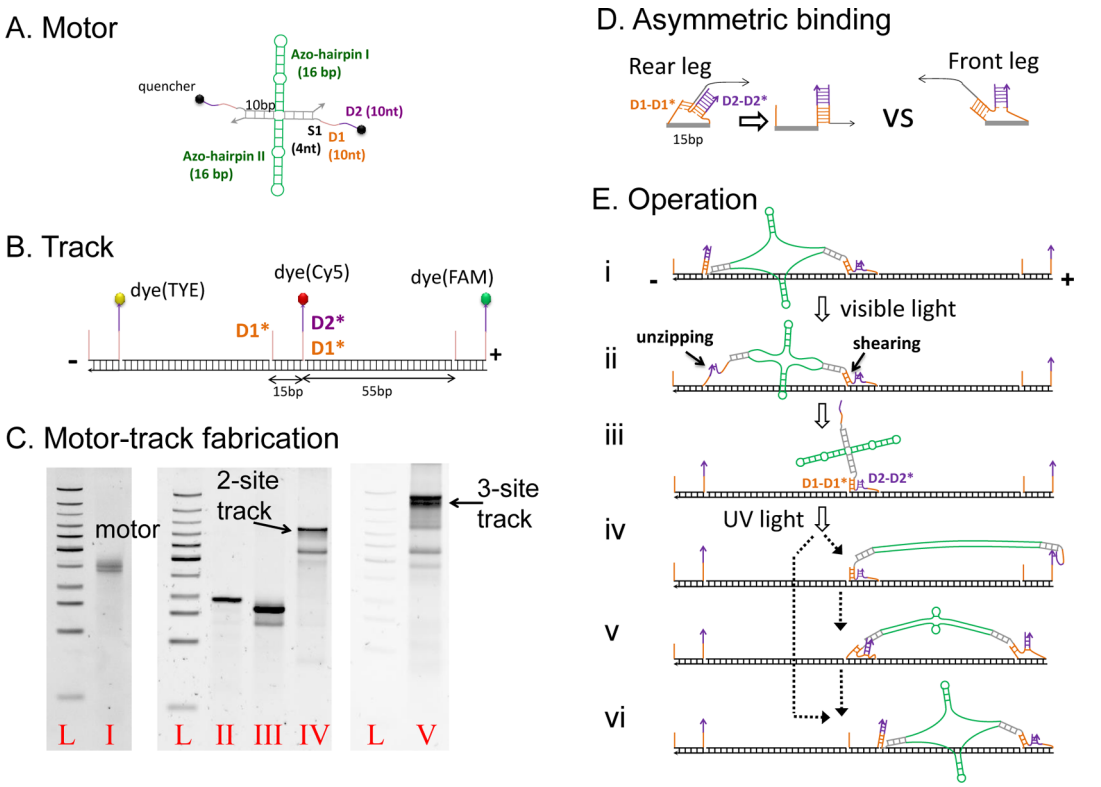

Figure 2. A bipedal DNA motor implementing a best regime (R3) of the design principle. (A,B) Construction of the motor and track. The nanomotor has two identical single-stranded legs and a pair of interleg hairpins capable of light-powered extension−contraction. The motor is made of two DNA strands embedded with light-responsive azobenzene moieties; the track is a long template strand hybridized with three strands for binding sites, and with two more strands for intersite spacers (arrow along a DNA strand for 3′ end, "nt" for nucleotides and "bp" for base pairs). D1*, D2* in the binding sites are complementary sequences to the leg sequences D1, D2. The track is labeled with fluorescent dyes site-specifically, and the motor is labeled with quenchers (BHQ-1) for characterization. (C) Gel images obtained using native PAGE (polyacrylamide gel electrophoresis) of the fabricated motor and tracks. Lanes L are DNA ladders. Lanes I, V are the annealed products for the motor and the three-site track. Lanes II−IV show stepwise assembly of a truncated two-site track (Lane II is truncated template, III is the annealed product of the template with the 55-nt spacer strand, IV is the full track). (D) Asymmetric leg-track binding. Schematically illustrated are the motor's rear and front legs under opposite pulling by the interleg bridge. The rear leg is dissociated along the forward edge of the binding site (corresponding to the less steep edge in Figure 1A) and the front leg along the backward edge (the steeper edge), hence preferential rear leg dissociation. (E) Possible states of the DNA motor under alternating visible and UV irradiation. States ii−v may be matched to states B1, C1, C2, B2 of regime R3 in Figure 1B (states ii, iii for a contracted mode; iv, v for an expulsive mode).

The contracted mode subjects the rear leg to a forward pull to break its D1-D1* duplex preferentially (Figure 2E, panel i). The remaining duplex is readily unzipped base-by-base by the motor's inward tension generated by the double-hairpin engine, while a simultaneous shearing of multiple base pairs is required to break the D1-D1* duplex at the front leg (panel ii). Indeed it is well-known that the shearing force is nearly two times[40] the unzipping force.

Hence the visible irradiation dissociates the rear leg preferentially (panel iii). An ensuing UV irradiation opens the two hairpins to release two antiparallel strands (each ∼54-nt long, including 12 azo-moieties that add to the backbone length similar[37] to extra nucleotides). With noncomplementary sequences the two strands cannot form a standard B-DNA helix. But their close proximity allows many hydrogen bonds to form, likely leading to an unconventional DNA duplex of unknown extension (probably longer than B-DNA helices). If the UV-switched engine reaches an extension equivalent of ∼2.5 turns of standard helices, the motor is near a relaxed mode for the dissociated leg to form the D2-D2* duplex at the front or back site. The motor then realizes regime R1 under repeated alternating visible-UV irradiations. If the UV-switched engine reaches an extension equivalent of 4 helical turns or more, the motor's bridge (engine plus two 10-bp spacers and two 4-nt linkers) is beyond the binding site period (70 bp). If the motor is so long that it bends to approach the back site from the outer, steeper edge for the D2-D2* duplex formation, the dissociated leg will bind the front site preferentially over the nearer back site (panels iv, v). The motor then accesses the expulsive mode, and realizes regime R3 under alternating visible-UV irradiations. A preferred forward binding is possible too if the track-bound leg is dragged forward to the less steep edge by the growing D2-D2* duplex (panel vi). Whether the motor can access R1 or a better regime depends on unknown size of an unconventional DNA structure, and can only be answered by experiments at this stage.

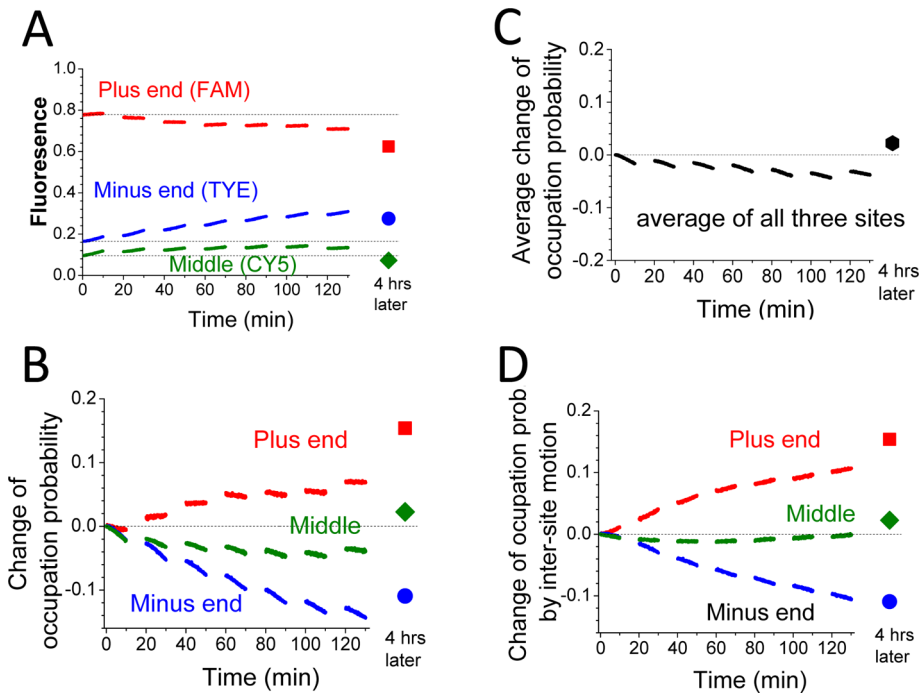

Figure 3. Plus-end directed motility of the motor along a three-site track. (A) Fluorescence from an equimolar mix of motor-track sample under six cycles of alternating visible light and UV irradiations (10 min per irradiation). Shown is the fluorescence signal calibrated against a bare-track control experiment for the same operation. The blank intervals are the time of UV irradiations when no fluorescence is collected. (B–D) The change of occupation probability for the three binding sites of the track extracted from the fluorescence in panel A. The symbols are the data obtained after a 4 h incubation of the operated sample. The occupation change directly attributed to the motor's intersite motion is shown in panel D, which is obtained by subtracting the data in panel B by those in panel C.

Computational Support for the Asymmetric Binding. We ran the oxDNA[41] package to simulate evolution of a leg-site binding under a forward or backward pull through the leg's D1 segment. The leg initially forms D1-D1* and D2-D2* duplexes with both overhangs of the site. 40 runs of simulations (~380 ns evolution time per run) are done for each of the three scenarios: forward pull of 9.7 pN, backward pull of the same force, and no pull. The simulations yield 5.7, 0.6 and 1.7 bp, respectively, for the average number of extra base pairs added to the D2-D2* duplex at the end of the simulations. The results support acceleration and deceleration of D1-D1* breaking by the forward and backward pull respectively, hence the binding asymmetry.

Fluorescence Measurement of Motor Motility. The motor's motion under the irradiation operation is monitored by detecting the fluorescence of different dyes that are tethered to the track site-specifically and subject to quenching by the motor-carried quenchers. Incubated motor-track samples of equilibrated motor-track binding (verified by constant fluorescence) are used for the operation experiments so that the motor's motion toward the plus end is signaled by a dropping fluorescence from the plus-end dye and a concomitant rising fluorescence from the minus-end dye. Each operation experiment on a motor-track mix is accompanied by a control experiment in which the same irradiation operation is applied to an equal amount of bare tracks without any motor. The fluorescence of the operated motor-track mix divided by that of the bare tracks is the real signal for the motor's operation largely free of dye optics. Such a control-calibrated fluorescence yields reliable information on site occupation by the motor and its binding/dissociation preference by further exploiting the nearly 100% efficiency[42] of contact quenching for the present motor (Materials and Methods).

Plus-End Directed Motion of the Motor. Figure 3A shows the control-calibrated fluorescence signal of the motor operating on a three-site track for six visible-UV irradiation cycles. The fluorescence from the plus and minus ends drops and rises respectively, signifying a net transfer of the motor's population from the minus end to the plus end. Figure 3B shows the increasing occupation probability at the plus end and the decreasing probability at the minus end. The occupation probability change averaged over the plus, minus and middle sites decreases with the operation cycles and flattens at a low value (~ −5%) (Figure 3C), suggesting that the motor mostly remains on the track during the operation-induced motion. The average occupation decrease is caused not by the entire derailment of the motor off track but by the operation-induced transition from two-leg binding states to single-leg states, because the operation cannot further derail the motor from a single-leg state due to the engine-leg separation.

The ~5% average decrease of occupation probability is recovered by a 4 h incubation of the sample after the six-cycle operation. The recovery occurs for all the three sites as their fluorescence all drops over the postoperation incubation (Figure 3A). This postoperation recovery is largely due to an incubation-induced recovery of the *trans*−*cis* ratio of the azo-moieties back to the preoperation, equilibrated value. Because the directional transfer of the motor's population should be evaluated against the equilibrated motor-track sample before the operation, the fluorescence signals immediately after the operation underestimate the motor's plus-end accumulation and overestimate the minus-end decumulation (Figure 3B). The real occupation change at each site caused by the motor's intersite motion is obtained by subtracting the average change during the operation. The results better match the postincubation signals, which show >10% occupation increase and decrease at the plus and minus ends, and a near-zero change at the middle site (Figure 3D).

The motor's speed is not directly measured in the ensemble fluorescence experiments, but has to be deduced from the fluorescence data in a model-dependent way. Realistic dynamic modeling of DNA motors remains difficult; a previous attempt[17] reports qualitative but not quantitative agreement with experiments. A rough comparison of the plus-end fluorescence drop induced by this motor and by another light-driven DNA motor[17] on a similar three-site track suggests comparable speeds for this motor and the previous one. The upper limit for the present motor is one forward step per irradiation cycle, but its real speed is apparently lower than the upper limit. The three-site track used in this study supports two consecutive steps of the motor maximally, since the motor might start from a single-leg state at the minus end prior to the operation (under visible light). However, the motor is potentially able to make many consecutive steps on a longer track as suggested by the observed low derailment. The motor's potential for long consecutive run length is largely due to its engine-leg separation as discussed above.

Directional Preference for Leg Binding. The motor's leg binding is induced by a UV irradiation that drives a transition from a single-leg state to a two-leg state. For the motor's operation on the three-site track, the fluorescence signals before and after a UV irradiation from the plus and minus ends yield the rate ratio for forward and backward binding of the dissociated leg of the single-leg state at the middle site. The rate ratio extraction is free of any complication from the single-leg states at the plus-end and minus-end sites as the leg binding from both states affects only the fluorescence from the middle site. The extracted ratio indicates a higher rate for forward binding than backward binding for all the six irradiation cycles (Figure 4A). The preference for the forward binding decreases with

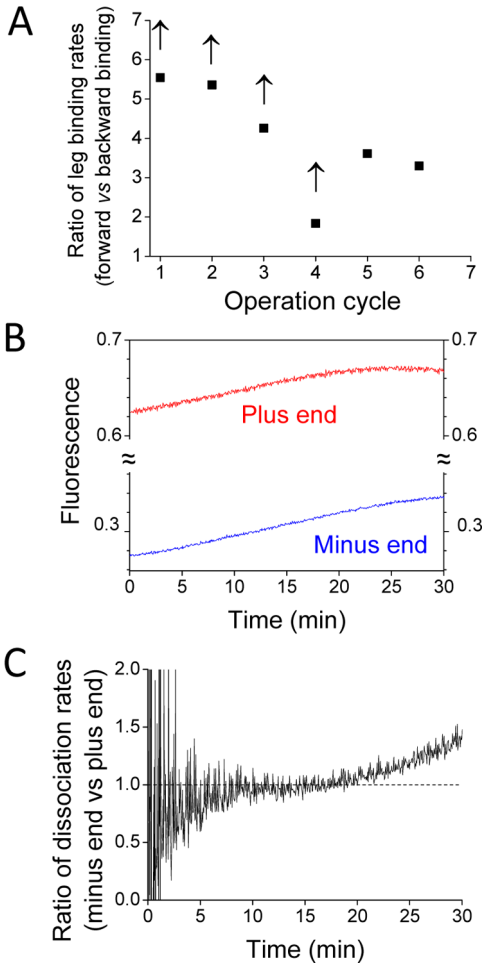

Figure 4. Directional biases of the motor on the three-site track. (A) Rate ratio of UV-induced leg binding to the plus-end site over the minus-end site from the operation experiment of Figure 3. The shown ratio per cycle is for the average binding rates during a cycle's UV irradiation, which are estimated from the control-calibrated fluorescence data immediately before and after the UV irradiation. Since the fluorescence drop from the minus-end dye is near zero for the first four cycles (see the data in Figure 3A), this would yield an infinite ratio. We instead use the average of the larger fluorescence drop of the other two cycles to estimate a lower ratio limit for the first four cycles (indicated by upward arrows). (B) The control-calibrated fluorescence signal over a single elongated visible light irradiation (30 min, done 4 h after the six-cycle operation experiment of Figure 3). (C) Rate ratio of leg dissociation from the minus-end site over the plus-end site estimated from the data in panel B. The shown ratio is for the average dissociation rates from the start of the visible irradiation to a later time as indicated by the time axis.

consecutive cycles; the same trend was previously observed for another bipedal DNA motor[17] in a similar ensemble fluorescence measurement. In both cases, the motor moves on short tracks containing a few binding sites. The operation cycles send the motor to the plus end where the motor becomes stalled and does not contribute to the forward bias signal anymore. But the available motor population supplying the plus end and contributing to the signal is reduced, hence the observed decrease of the bias signal in this

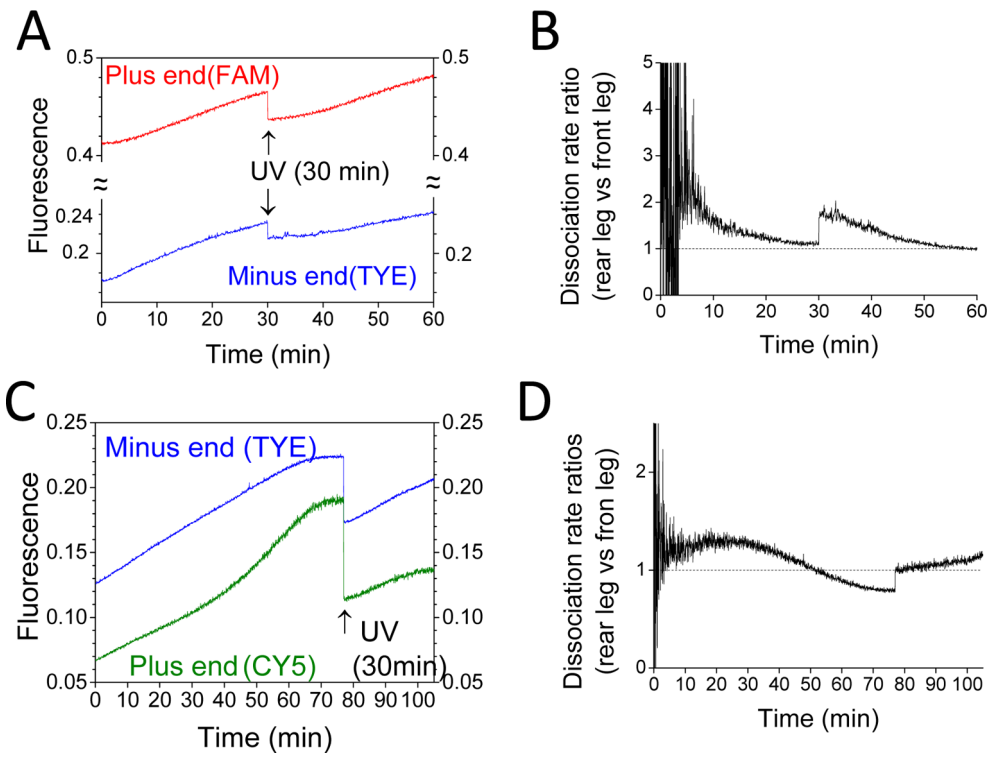

Figure 5. Directional biases of the motor on truncated two-site tracks under an elongated single-cycle operation. (A) Control-calibrated fluorescence signal for a two-site track labeled with dyes FAM and TYE. The operation is a 30 min visible light irradiation plus a 30 min UV irradiation. The fluorescence was collected before and after the UV irradiation. (B) Dissociation rate ratio estimated from the fluorescence data in panel A. The shown ratio is for the average dissociation rates from the start of the operation to a later time as indicated by the time axis. (C,D) The same as panels A and B but for different dye labeling (CY5, TYE) and a longer visible light irradiation (77 min).

study. The motor's real forward bias does not necessarily decrease when the motor moves on a long track with the same periodic binding sites.

Directional Preference for Leg Dissociation. The motor's leg dissociation is induced by a visible light irradiation that drives a transition from a two-leg state to a single-leg state. For the motor's operation on the three-site track, the fluorescence signals from the plus and minus ends collected during an elongated visible irradiation indicate a higher rate for leg dissociation from the minus end than the plus end (Figure 4B,C). We note that the detected dissociation events at the two sites are from different two-leg bound motors on the three-site track.

To detect any leg dissociation preference for the same motor, we conduct operation experiments on truncated two-site tracks in which the dissociation events at the plus and minus end are unambiguously related to the same motor's front and rear legs. To better expose any preference, a single-cycle operation of elongated visible and UV irradiations is applied. The data show clearly a higher dissociation rate for the rear leg than the front leg for the same motor (Figure 5).

Dissociation and Binding Preferences Independent of Fluorescent Labels. The signals for both preferences are based on the control-calibrated fluorescence that largely removes any dependence on optical properties of the used dyes. As a further confirmation, the single-cycle operation experiments are done for two different dye labeling schemes: the initial quenching is higher for the minus end than the plus end in one case (Figure 5A), but becomes opposite in another case (Figure 5C), yet the same preference for rear leg dissociation is observed in both cases (Figure 5B,D). Besides, the single-cycle operation experiments in both cases show that the UV-induced decrease of the control-calibrated fluorescence signal is more for the plus end than the minus end, further confirming the preference for forward leg binding (Figure 5A,C).

Dependence on Light Operation. A completely parameter-free comparison of the motor's performance for different durations of the visible and UV irradiations may be done for a track labeled with multiple dyes using the percentage change of control-calibrated fluorescence signals against the initial preoperation signals of the equilibrated motor-track mix. Following a previous study,[17] the percentage change of the minus-end dye minus that of the plus-end dye reflects the motor's directional intersite motion, and the average of percentage change over all dyes on the track reflects leg dissociation. The direction and dissociation signals thus defined are obtained for both three-site and two-site tracks for different irradiation durations (Figure 6). The signals are not the absolute magnitude of the

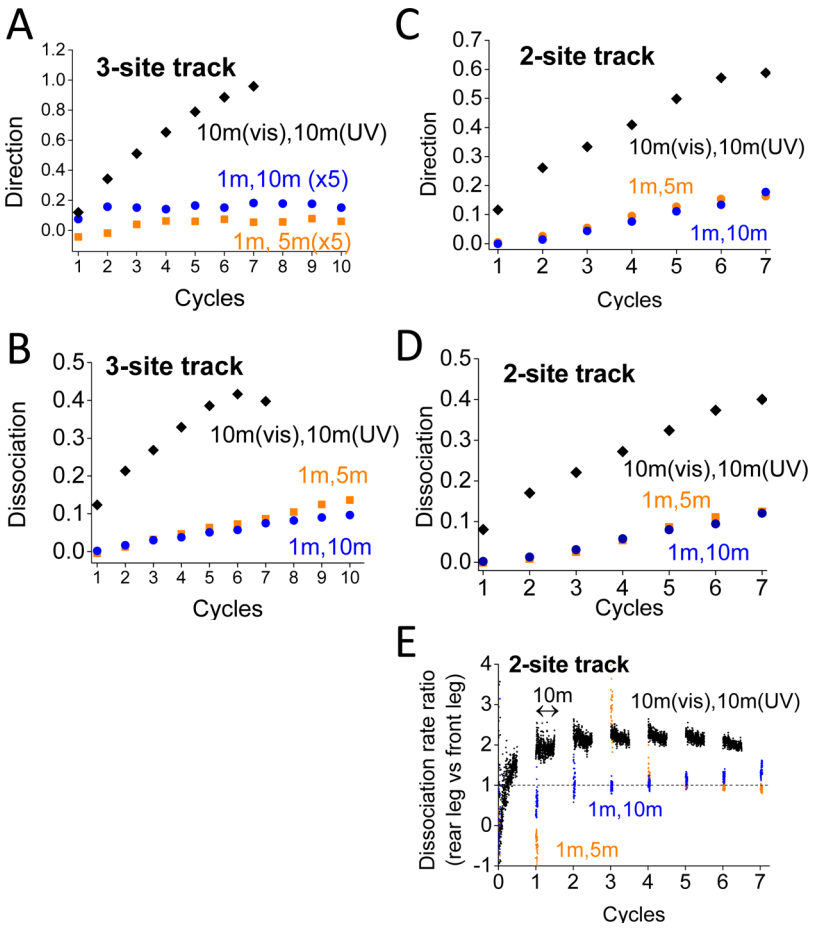

Figure 6. Motor performance *versus* varied irradiation duration. The direction and dissociation signals are obtained in a parameter-free way from the percentage fluorescence change of the track-tethered dyes against their preoperation fluorescence (*i.e.*, $\Delta I_M/I_{M0} = (I_M - I_{M0})/I_{M0}$, with I_{M0}, I_M being a dye's fluorescence at the start of an operation experiment and immediately after a visible-UV irradiation cycle. I_{M0}, I_M are both calibrated against the bare-track control). The direction signal (panels A, C) is the percentage change for the minus-end dye minus that for the plus-end dye; the dissociation signal (panels B, D) is the average of the percentage changes for all the dyes on the track. The dissociation rate ratio in panel E is estimated in the same way as Figure 5. The two-site track producing the data in panels C, D, E are labeled with dyes CY5 and FAM at the minus and plus ends.

motor's direction and leg dissociation, but reflect the motor's relative performance under differing operation. The results show that the motor's direction and leg dissociation signals are both reduced drastically when the irradiation cycle is shortened from 10 min visible light and 10 min UV to 1 min visible light, and further to 5 min UV. Besides, the preference for rear leg dissociation is observed again for a third dye labeling scheme (Figure 6E). The dissociation rate ratio of the rear leg over the front leg rises and then flattens under consecutive cycles of irradiations. A similar pattern was previously reported for another DNA motor.[17]

DISCUSSION

The DNA Motor as a First Experimental Demonstration of the Modular Design Principle. The DNA bipedal motor evidently implements the two major requirements of the modular design: an interleg bridge containing an engine-like switchable component (hairpins) that is located distantly from the legs yet is able to dissociate the leg from the track; and a leg-track binding component that is asymmetric to allow preferential breaking along one direction of the track than the opposite direction. Leg dissociation and binding by the switched interleg hairpins are confirmed by the fluorescence rise and drop induced by the visible and UV irradiations, especially in the single-cycle experiments shown by Figure 5 (for two-site tracks) and Figure 4C (for three-site tracks). The asymmetric leg-track binding is confirmed straightforwardly by the preferential rear leg dissociation found for the motor on a two-site track (Figure 5, Figure 6E), because the two track-bound legs in this case are pulled by a force of equal magnitude but opposite direction when the interleg bridge is shortened by a visible light irradiation. Although the preference is quantitatively weak, the effect is qualitatively clear and underpins the signals for the motor's directional motion (Figure 3). Thus, we can conclude that the present motor achieves the modular design in that an optical switching operation

on a pair of hairpins but not directly on the leg-track binding dissociates the legs from a distance and makes a unidirectional bipedal motor.

Moreover, the motor also possesses a preference for forward leg binding as found for the motor operating on three-site and two-site tracks (Figure 4A, Figure 5A,C). The detailed molecular mechanisms are not clear at this stage, largely due to unknown length of an unconventional DNA structure that exists transiently under the UV irradiation. Nevertheless, the observed signals for the binding preference suggest that the motor achieves a best regime of the modular design principle.

Characters of the Modular Design Principle. The present DNA motor exemplifies some characters of the underlying design principle. First, the motor demonstrates a molecular mechanism that rectifies back-and-forth extension/contraction inside the motor into its sustained directional motion. This character differentiates the present motor from all previously reported artificial track-walking nanomotors. Second, the motor and its underlying design principle also differ from previous theoretical proposals[43−47] of nanomotors by length change: the latter are all inchworm motors moving either forward or backward along the motor's initial orientation; the former are hand-over-hand motors of a unidirectionality intrinsically decided by motor-track binding asymmetry. Third, the design principle allows integration of a bias for rear leg dissociation and a bias for ensuing leg binding forward. This mechanistic integration is important for a motor to gain a high directional fidelity[39,48,49] (*i.e.*, high chance of successful forward motion per operation) and a high efficiency.[50] How to implement directional biases[17,51−58] is a central problem in the development of nanomotors in general. Fourth, no damage of the track in wake of a motor's motion (*i.e.*, burn-the-bridge method) is required to rectify the motor's direction. Overall, the modular design principle leads to a new class of nanomotors.

A Divide-and-Conquer Strategy to Lower the Technical Barrier for Nanomotor Development. Multiple regimes exist for implementing the modular design principle up to various levels of mechanistic integration and performance. Two major technical requirements shared by all the regimes are an asymmetric binding mechanism for motion control and a bistate contraction−extension switch for energy consumption and force generation. The two components need not be done by a single molecular part as for previous motors; they instead may be separately implemented and optimized into "modular" molecular parts, and then assembled flexibly into nanomotors of many versions. This amounts to a "divide and conquer" strategy that is expected to lower the technical difficulty for nanomotor development and render this by-far small and difficult field accessible to the much larger community of nanodevice researchers. The engine-like switch may be done by polymer winding or expulsion, by switch of contour length or rigidity, by means of light,[24,25,28,34,37] PH change,[23,35] temperature change,[30,33] chemical stimuli,[22,26,27,31] molecular binding[29,32,36,38] *etc.*; many of these methods are already demonstrated in devices built from DNA, peptides or synthetic polymers. The asymmetric binding has been demonstrated in many devices[11,16,17] too. Other candidates for the switch and binding modules are many proteins that are known for asymmetric binding[59,60] with DNA helices or protein filaments, and for modulating[61,62] length/rigidity of peptides and DNA. Following the present design principle, new nanomotors might be constructed from some of the switching and binding modules. This might lead to new DNA motors, protein motors or motors of synthetic polymers from switching and binding modules of the same molecular type for sake of compatibility. Hybrid motors are possible too, *e.g.*, by use of DNA-binding proteins and covalent protein−DNA linkages.[63] Therefore, the modular design principle potentially enables a big variety of nanomotors with rich variations in molecular systems (DNA, proteins, synthetic polymers or their hybrids) and driving methods (light, fuels, PH change, ligand binding, *etc.*).

The modular design principle also offers some advantages for improving nanomotor performance. With the engine-leg separation, a common engine may drive dissimilar motors, and a certain leg-track combination befits multiple interchangeable engines. This versatility might help motors to access different working regimes of the design principle for a better performance. For example, the leg and track of the present DNA motor might be combined with a previously reported DNA duplex−quadruplex switch[29] for a new motor of different performance, although the specific leg-track binding is not easily integrated with switches of protein or synthetic polymers. Besides, the engine-leg separation of the present motor potentially allows it to make many consecutive runs on a longer track, because the energy consumption (*i.e.*, light operation) does not weaken a track-bound leg after the other leg's dissociation like other reported bipedal motors. This renders the present motor a suitable candidate for applications involving long-range transport, a possibility worth future study.

CONCLUSION

We have proposed a new design principle for track-walking nanomotors and provided a first experimental demonstration by implementing the design principle in a light-powered symmetric DNA bipedal nanomotor. As exemplified by the motor, the design principle allows modularized assembly of self-directed and self-propelled nanomotors from spatially and functionally separated engine-like bistate switch motifs and leg-like binding motifs, and up to mechanistic sophistication necessary for high-performing nanomotors. The modular design principle possesses rich variations

for implementation and presents a viable route to develop a big class of new nanomotors from numerous molecular switches and binding motifs from the fields of nanodevices and molecular biology.

MATERIALS AND METHODS

DNA Strands and Sequences. The motor is made of two 97-bp strands: MS1 = BHQ-1-5′-S3-D2-D1-S1-B1-H1-B2-S2-3′ and MS2 = BHQ-1-5′-S3-D2-D1-S1-B2*-H2-B1*-S2-3′ with the asterisk marking complementary sequences. The strands each contain a 20-nt leg segment (D2-D1), a 42-nt hairpin embedded with 12 azo-moieties in the nucleotide backbone, two 10-nt segments (B1, B2) for double-stranded spacers separating the leg and hairpin, and three linker segments (S1, S2, S3 of 4, 9, and 2 nt, respectively) for flexibility. Below are the nucleotide sequences for the segments (from 5′ to 3′):

D1 = TGGAATGACT, D2 = GTGATTGTAG;

S1 = ACCA, S2 = ATGTCGCCT, S3 = CC;

B1 = ATGGACGATC, B2 = CGCATGCTAG;

H1 = CTXTTXAAXGA(TTT)CTXTTXAAXGA(TTTT)TXCTX-TAXAAG(TTT)TXCTXTAXAAG;

H2 = GAAXATXTCXT(TTT)GAAXATXTCXT(TTTT)AGXAAX-TTXTC(TTT)AGXAAXTTXTC (X represents azo-moieties; brackets mark loop sequences of the hairpins).

The three-site track is made of three strands for binding sites (TS1, TS2, TS3, 45 bp each, carrying dyes TYE, CY5 and FAM, respectively), two identical spacer strands (TS4, 55 bp) and a long template (TS5, 155 bp). Below are the sequences for the strands (from 5′ to 3′):

TS1 = 5′-D1*-B3*-D1*-D2*+TYE with B3* = CAACAGCAAT-GTTCG;

TS2 = 5′-D1*-B4*-D1*-D2*+CY5 with B4* = TTACAATCCG-TCGTG;

TS3 = 5′-D1*-B5*-D1*-D2*+FAM with B5* = AGCGATTACT-TGTGC;

TS4 = 5′-B6*-3′ with

B6* = AGCTAGTCCAAGGGGATCGTAGTATTTTGCATGACA-AAGCCCCAGCCATTATAGC;

TS5 = 5′-B5-B6-B4-B6-B3-3′.

The two-site tracks use a short template truncated from TS5 as 5′-B5-B6-B4-3′, 5′-B5-B6-B3-3′ or 5′-B4-B6-B3-3′. The resultant tracks carry two dyes, namely, CY5-FAM, TYE-FAM, or TYE-CY5, respectively, from minus to plus end.

Motor-Track Fabrication. The methods for motor-track assembly and gel analysis largely follow our previous studies on DNA motors (see refs 16, 17 for details). The DNA strands are purchased from commercial suppliers (azobenzene-tethered strands from Nihon Techno Service Co., Ltd., other strands from Integrated DNA Technologies, Inc.) To assemble the tracks, the strands were mixed stoichiometrically in a buffer containing 1.5 M NaCl, 10 mM Tris, 1 mM EDTA buffer (pH 8). The mixed sample was annealed at 95 °C for 20 min, and then cooled down to 25 °C over 4 h. The motor was assembled by the same annealing procedure in the same buffer (except for 2 M of NaCl). The annealing products were analyzed in a 10% native PAGE gel against a low molecular weight DNA Ladder (purchased from New England BioLabs, Inc., with 25-bp and 766-bp as the lowest and highest band, respectively).

Operation Experiments. The motor-track mix was incubated 12 h before an operation experiment. Both the incubation and later operation were done at 25 °C in a buffer containing 15 mM sodium acetate, 9.5 mM Tris, 1 mM EDTA. The motor/track concentration was kept low (~5 nM) for all the operation experiments shown in this study to suppress possible cross-linking of multiple tracks by a motor. The irradiation operation and fluorescence measurement were both done using a RF-5301PC spectrophotometer (150 W xenon lamp, Shimadzu Corp.). For each round of irradiation operation, the motor-track sample was first irradiated by visible light for a defined duration (kinetic mode scanning wavelengths 495 nm, 549 nm, 648 nm over 5 nm slit width each) followed by another period of UV irradiation (360 nm over 5 nm slit width). The fluorescence was collected during the visible irradiation, which was also the excitation for the three dyes (excitation/emission wavelengths: 495 nm/520 nm for FAM, 549 nm/563 nm for TYE, 648 nm/668 nm for Cy5).

Computer Simulation of Binding Asymmetry. The software used is a simulation package based on a coarse-grained DNA model (see ref 41 for details). The simulation was done for a leg (45-nt D1-D2 segment) bound with the middle binding site with the latter located at the middle of a 25-bp duplex truncated of the track backbone. To exert a pulling force to the leg with the track at rest, we applied two harmonic traps to immobilize the two terminal nucleotides of the truncated template strand. The traps are 7.6 nm apart to match the 25-bp track (with an elastic constant of 5.7 pN/nm). A Monte Carlo simulation was done to construct an initial configuration in which the D2-D2* duplex and the noncontiguous D1-D1* duplex are fully hybridized. Then a Langevin dynamics was used to evolve the configuration (15 fs per step). Both the Monte Carlo and Langevin dynamic simulations were done for room temperature relevant to the experiments.

Extracting Occupation Probability and Rate Ratios from the Fluorescence Data. Following a previous study,[17] the probability for a site to be occupied by a motor is related to the fluorescence of the dye tethered to the site as $P(t) = [1 - I_{MT}(t)/I_T(t)]/\gamma$. Here $I_{MT}(t)$ is the fluorescence collected from an operated motor-track sample at a time t, $I_T(t)$ is the fluorescence of an equal amount of bare tracks from the accompanying control experiment. γ is the quenching efficiency of the dye by the motor-carried quencher. Hence the control-calibrated fluorescence $I_M(t) = I_{MT}(t)/I_T(t)$ yields the probability as $P(t) = [1 - I_M(t)]/\gamma$. The average rate for leg dissociation from time t_1 to a later time t_2 is $k_d = [P(t_1) - P(t_2)]/(t_2 - t_1) = [I_M(t_2) - I_M(t_1)]/\gamma(t_2 - t_1)$. The rate ratio for leg dissociation from the minus-end site over the plus-end site is $k_{d-}/k_{d+} = (\gamma_+/\gamma_-) \times [I_{M-}(t_2) - I_{M-}(t_1)]/[I_{M+}(t_2) - I_{M+}(t_1)]$, in which (+) and (−) mark the plus and minus ends. Similarly, the average rate for leg binding from t_1 to t_2 is $k_{b\pm} = [P_\pm(t_2) - P_\pm(t_1)]/(t_2 - t_1) = [I_{M\pm}(t_1) - I_{M\pm}(t_2)]/\gamma_\pm(t_2 - t_1)$. The rate ratio for leg binding to the plus-end site over the minus-end site is $k_{b+}/k_{b-} = (\gamma_-/\gamma_+) \times [I_{M+}(t_1) - I_{M+}(t_2)]/[I_{M-}(t_1) - I_{M-}(t_2)]$. The leg-track binding of the present motor ensures a contact quenching of near 100% quenching efficiency[42] for the three dyes used, *i.e.*, $\gamma \approx 1$ and $\gamma_+/\gamma_- \approx 1$ for a good approximation. Thus, the probability $P(t)$ and rate ratios k_{d-}/k_{d+}, k_{b+}/k_{b-} can be extracted directly from $I_M(t)$. The control-calibrated fluorescence also removes any influence of photobleaching (a slight effect for the present motor).

Conflict of Interest: The authors declare no competing financial interest.

Acknowledgment. This work is partially supported by FRC grants under R-144-000-290-112, R-144-000-320-112 (to Z. S. Wang) and MOE tier 2 grant under R-144-000-325-112 (to Z. S. Wang). We thank A. A. Louis, J. P. K. Doye, T. E. Ouldridge for kind permission to use the oxDNA package.

REFERENCES AND NOTES

1. Gu, H.; Chao, J.; Xiao, S.-J.; Seeman, N. C. A Proximity-Based Programmable DNA Nanoscale Assembly Line. *Nature* **2010**, *465*, 202–205.
2. Lund, K.; Manzo, A. J.; Dabby, N.; Michelotti, N.; Johnson-Buck, A.; Nangreave, J.; Taylor, S.; Pei, R.; Stojanovic, M. N.; Walter, N. G.; *et al.* Molecular Robots Guided by Prescriptive Landscapes. *Nature* **2010**, *465*, 206–210.
3. He, Y.; Liu, D. R. Autonomous Multistep Organic Synthesis in a Single Isothermal Solution Mediated by a DNA Walker. *Nat. Nanotechnol.* **2010**, *5*, 778–782.
4. Lewandowski, B.; Bo, G. D.; Ward, J. W.; Papmeyer, M.; Kuschel, S.; Aldegunde, M. J.; Gramlich, P. M. E.; Heckmann,

D.; Goldup, S. M.; D'Souza, D. M.; *et al.* Sequence-Specific Peptide Synthesis by an Artificial Small-Molecule Machine. *Science* **2013**, *339*, 189–193.
5. Kay, E. R.; Leigh, D. A.; Zerbetto, F. Synthetic Molecular Motors and Mechanical Machines. *Angew. Chem., Int. Ed.* **2007**, *46*, 72–191.
6. Sherman, W. B.; Seeman, N. C. A Precisely Controlled DNA Biped Walking Device. *Nano Lett.* **2004**, *4*, 1203–1207.
7. Shin, J. S.; Pierce, N. A. A Synthetic DNA Walker for Molecular Transport. *J. Am. Chem. Soc.* **2004**, *126*, 10834–10835.
8. Yin, P.; Yan, H.; Daniell, X. G.; Turberfield, A. J.; Reif, J. H. A Unidirectional DNA Walker That Moves Autonomously along a Track. *Angew. Chem., Int. Ed.* **2004**, *43*, 4906–4911.
9. Bath, J.; Green, S. J.; Turberfield, A. J. A Free-Running DNA Motor Powered by a Nicking Enzyme. *Angew. Chem., Int. Ed.* **2005**, *44*, 4358–4361.
10. Tian, Y.; He, Y.; Chen, Y.; Yin, P.; Mao, C. A DNAzyme That Walks Processively and Autonomously along a One-Dimensional Track. *Angew. Chem., Int. Ed.* **2005**, *44*, 4355–4358.
11. Green, S.; Bath, J.; Turberfield, A. Coordinated Chemomechanical Cycles: A Mechanism for Autonomous Molecular Motion. *Phys. Rev. Lett.* **2008**, *101*, 238101(1−4).
12. Bath, J.; Green, S. J.; Allen, K. E.; Turberfield, A. J. Mechanism for a Directional, Processive, and Reversible DNA Motor. *Small* **2009**, *5*, 1513–1516.
13. Omabegho, T.; Sha, R.; Seeman, N. C. A Bipedal DNA Brownian Motor with Coordinated Legs. *Science* **2009**, *324*, 67–71.
14. Von Delius, M.; Geertsema, E. M.; Leigh, D. A. A Synthetic Small Molecule That Can Walk down a Track. *Nat. Chem.* **2009**, *2*, 96–101.
15. You, M.; Chen, Y.; Zhang, X.; Liu, H.; Wang, R.; Wang, K.; Williams, K. R.; Tan, W. An Autonomous and Controllable Light-Driven DNA Walking Device. *Angew. Chem., Int. Ed.* **2012**, *51*, 2457–2460.
16. Cheng, J.; Sreelatha, S.; Hou, R.; Efremov, A.; Liu, R.; van der Maarel, J. R. C.; Wang, Z. Bipedal Nanowalker by Pure Physical Mechanisms. *Phys. Rev. Lett.* **2012**, *109*, 238104.
17. Liu, M.; Hou, R.; Cheng, J.; Loh, I. Y.; Sreelatha, S.; Tey, J. N.; Wei, J.; Wang, Z. Autonomous Synergic Control of Nanomotors. *ACS Nano* **2014**, *8*, 1792–1803.
18. Tierney, H. L.; Murphy, C. J.; Jewell, A. D.; Baber, A. E.; Iski, E. V.; Khodaverdian, H. Y.; McGuire, A. F.; Klebanov, N.; Sykes, E. C. H. Experimental Demonstration of a Single-Molecule Electric Motor. *Nat. Nanotechnol.* **2011**, *6*, 625–629.
19. Vale, R. D.; Milligan, R. A. The Way Things Move: Looking Under the Hood of Molecular Motor Proteins. *Science* **2000**, *288*, 88–95.
20. Yildiz, A.; Forkey, J. N.; McKinney, S. A.; Ha, T.; Goldman, Y. E.; Selvin, P. R. Myosin V Walks Hand-Over-Hand: Single Fluorophore Imaging with 1.5-nm Localization. *Science* **2003**, *300*, 2061–2065.
21. Cross, R. A. Molecular Motors: Dynein's Gearbox. *Curr. Biol.* **2004**, *14*, R355–R356.
22. Anelli, P. L.; Spencer, N.; Stoddart, J. F. A Molecular Shuttle. *J. Am. Chem. Soc.* **1991**, *113*, 5131.
23. Bissell, R. A.; Córdova, E.; Kaifer, A. E.; Stoddart, J. F. A Chemically and Electrochemically Switchable Molecular Shuttle. *Nature* **1994**, *369*, 133–137.
24. Murakami, H.; Kawabuchi, A.; Kotoo, K.; Kunitake, M.; Nakashima, N. A Light-Driven Molecular Shuttle Based on a Rotaxane. *J. Am. Chem. Soc.* **1997**, *119*, 7605–7606.
25. Brouwer, A. M.; Frochot, C.; Gatti, F. G.; Leigh, D. A.; Mottier, L.; Paolucci, F.; Roffia, S.; Wurpel, G. W. H. Photoinduction of Fast, Reversible Translational Motion in a Hydrogen-Bonded Molecular Shuttle. *Science* **2001**, *291*, 2124–2128.
26. Marlin, D. S.; Cabrera, D. G.; Leigh, D. A.; Slawin, M. Z. An Allosterically Regulated Molecular Shuttle. *Angew. Chem., Int. Ed.* **2006**, *45*, 1385–1390.
27. Jiménez, M. C.; Dietrich-Buchecker, C.; Sauvage, J.-P. Towards Synthetic Molecular Muscles: Contraction and Stretching of a Linear Rotaxane Dimer. *Angew. Chem., Int. Ed.* **2000**, *39*, 3284–3487.
28. Hugel, T.; Holland, N. B.; Cattani, A.; Moroder, L.; Seitz, M.; Gaub, H. E. Single-Molecule Optomechanical Cycle. *Science* **2002**, *296*, 1103–1106.
29. Alberti, P.; Mergny, J.-L. DNA Duplex−quadruplex Exchange as the Basis for a Nanomolecular Machine. *Proc. Natl. Acad. Sci. U. S. A.* **2003**, *100*, 1569–1573.
30. Azov, V. A.; Schlegel, A.; Diederich, F. Geometrically Precisely Defined Multinanometer Expansion/Contraction Motions in a Resorcin[4]arene Cavitand Based Molecular Switch. *Angew. Chem., Int. Ed.* **2005**, *44*, 4635–4638.
31. Liu, Y.; Flood, A. H.; Bonvallet, P. A.; Vignon, S. A.; Northrop, B. H.; Tseng, H.-R.; Jeppesen, J. O.; Huang, T. J.; Brough, B.; Baller, M.; *et al.* Linear Artificial Molecular Muscles. *J. Am. Chem. Soc.* **2005**, *127*, 9745–9759.
32. Lubrich, D.; Lin, J.; Yan, J. A Contractile DNA Machine. *Angew. Chem., Int. Ed.* **2008**, *47*, 7026–7028.
33. Hamad-Schifferli, K.; Schwartz, J. J.; Santos, A. T.; Zhang, S.; Jacobson, J. M. Remote Electronic Control of DNA Hybridization through Inductive Coupling to an Attached Metal Nanocrystal Antenna. *Nature* **2002**, *415*, 152–155.
34. Mayer, G.; Kröck, L.; Mikat, V.; Engeser, M.; Heckel, A. Light-Induced Formation of G-Quadruplex DNA Secondary Structures. *ChemBioChem* **2005**, *6*, 1966–1970.
35. Liedl, T.; Simmel, F. C. Switching the Conformation of a DNA Molecule with a Chemical Oscillator. *Nano Lett.* **2005**, *5*, 1894–1898.
36. Xiao, Y.; Plakos, K. J. I.; Lou, X.; White, R. J.; Qian, J.; Plaxco, K. W.; Soh, H. T. Fluorescence Detection of Single-Nucleotide Polymorphisms with a Single, Self-Complementary, Triple-Stem DNA Probe. *Angew. Chem., Int. Ed.* **2009**, *48*, 1–6.
37. Liang, X.; Mochizuki, T.; Asanuma, H. A Supra-Photoswitch Involving Sandwiched DNA Base Pairs and Azobenzenes for Light-Driven Nanostructures and Nanodevices. *Small* **2009**, *5*, 1761–1768.
38. Vallée-Bélisle, A.; Ricci, F.; Plaxco, K. W. Thermodynamic Basis for the Optimization of Binding-induced Biomolecular Switches and Structure-Switching Biosensors. *Proc. Natl. Acad. Sci. U. S. A.* **2009**, *106*, 13802–13807.
39. Efremov, A.; Wang, Z. Maximum Directionality and Systematic Classification of Molecular Motors. *Phys. Chem. Chem. Phys.* **2011**, *13*, 5159–5170.
40. Kufer, S. K.; Puchner, E. M.; Gumpp, H.; Liedl, T.; Gaub, H. E. Single-Molecule Cut-and-Paste Surface Assembly. *Science* **2008**, *319*, 594–596.
41. Ouldridge, T. E.; Hoare, R. L.; Louis, A. A.; Doye, J. P. K.; Bath, J.; Turberfield, A. J. Optimizing DNA Nanotechnology through Coarse-Grained Modeling: A Two-Footed DNA Walker. *ACS Nano* **2013**, *7*, 2479–2490.
42. Marras, S. A. E.; Kramer, F. R.; Tyagi, S. Efficiencies of Fluorescence Resonance Energy Transfer and Contact-mediated Quenching in Oligonucleotide Probes. *Nucleic Acids Res.* **2002**, *30*, e122.
43. Porto, M.; Urbakh, M.; Klafter, J. Atomic Scale Engines: Cars and Wheels. *Phys. Rev. Lett.* **2000**, *84*, 6058–6061.
44. Wang, Z. Bioinspired Laser-Operated Molecular Locomotive. *Phys. Rev. E: Stat., Nonlinear, Soft Matter Phys.* **2004**, *70*, 031903.
45. Najafi, A.; Golestanian, R. Simple Swimmer at Low Reynolds Number: Three Linked Spheres. *Phys. Rev. E: Stat., Nonlinear, Soft Matter Phys.* **2004**, *69*, 062901.
46. Li, D.; Fan, D.; Wang, Z. General Mechanism for Inchworm Nanoscale Track Walkers: Analytical Theory and Realistic Simulation. *J. Chem. Phys.* **2007**, *126*, 245105–11.
47. Li, D.; Fan, D.; Zheng, W.; Le, Y.; Wang, Z. From Molecular Shuttles to Directed Procession of Nanorings. *Chem. Phys.* **2008**, *352*, 235–240.
48. Efremov, A.; Wang, Z. Universal Optimal Working Cycles of Molecular Motors. *Phys. Chem. Chem. Phys.* **2011**, *13*, 6223–6233.
49. Wang, Z.; Hou, R.; Efremov, A. Directional Fidelity of Nanoscale Motors and Particles Is Limited by the 2nd Law of Thermodynamics—*via* a Universal Equality. *J. Chem. Phys.* **2013**, *139*, 035105.
50. Hou, R.; Wang, Z. Role of Directional Fidelity in Multiple Aspects of Extreme Performance of the F1-ATPase Motor.

Phys. Rev. E: Stat., Nonlinear, Soft Matter Phys. **2013**, *88*, 022703.
51. Rousselet, J.; Salome, L.; Ajdari, A.; Prostt, J. Directional Motion of Brownian Particles Induced by a Periodic Asymmetric Potential. *Nature* **1994**, *370*, 446–448.
52. Faucheux, L. P.; Bourdieu, L. S.; Kaplan, P. D.; Libchaber, A. J. Optical Thermal Ratchet. *Phys. Rev. Lett.* **1995**, *74*, 1504–1507.
53. Linke, H.; Humphrey, T. E.; Löfgren, A.; Sushkov, A. O.; Newbury, R.; Taylor, R. P.; Omling, P. Experimental Tunneling Ratchets. *Science* **1999**, *286*, 2314–2317.
54. Hernández, J. V.; Kay, E. R.; Leigh, D. A. A Reversible Synthetic Rotary Molecular Motor. *Science* **2004**, *306*, 1532–1537.
55. Lee, S.-H.; Ladavac, K.; Polin, M.; Grier, D. G. Observation of Flux Reversal in a Symmetric Optical Thermal Ratchet. *Phys. Rev. Lett.* **2005**, *94*, 110601.
56. Wang, Z.; Feng, M.; Zheng, W.; Fan, D. Kinesin Is an Evolutionarily Fine-Tuned Molecular Ratchet-and-Pawl Device of Decisively Locked Direction. *Biophys. J.* **2007**, *93*, 3363–3372.
57. Wang, Z. Synergic Mechanism and Fabrication Target for Bipedal Nanomotors. *Proc. Natl. Acad. Sci. U. S. A.* **2007**, *104*, 17921–17926.
58. Cheng, J.; Sreelatha, S.; Loh, I. Y.; Liu, M.; Wang, Z. A Bioinspired Design Principle for DNA Nanomotors: Mechanics-Mediated Symmetry Breaking and Experimental Demonstration. *Methods* **2014**, *67*, 227–233.
59. Gebhardt, J. C. M.; Clemen, A. E.-M.; Jaud, J.; Rief, M. Myosin-V Is a Mechanical Ratchet. *Proc. Natl. Acad. Sci. U. S. A.* **2006**, *103*, 8680–8685.
60. Gennerich, A.; Carter, A. P.; Reck-Peterson, S. L.; Vale, R. D. Force-Induced Bidirectional Stepping of Cytoplasmic Dynein. *Cell* **2007**, *131*, 952–965.
61. Liu, Y.; Chen, H.; Kenney, L. J.; Yan, J. A Divalent Switch Drives H-NS/DNA-Binding Conformations between Stiffening and Bridging Modes. *Genes Dev.* **2010**, *24*, 339–344.
62. Fu, H.; Le, S.; Muniyappa, K.; Yan, J. Dynamics and Regulation of RecA Polymerization and De-Polymerization on Double-Stranded DNA. *PLoS One* **2013**, *8*, e66712.
63. Tse, Y. C.; Kirkegaard, K.; Wang, J. C. Covalent Bonds between Protein and DNA. Formation of Phosphotyrosine Linkage between Certain DNA Topoisomerases and DNA. *J. Biol. Chem.* **1980**, *255*, 5560–5565.